Micron 56 (2014) 17–28

Contents lists available at ScienceDirect

Micron

journal homepage: www.elsevier.com/locate/micron

# A novel algorithm based on visual saliency attention for localization and segmentation in rapidly-stained leukocyte images

Xin Zheng, Yong Wang, Guoyou Wang*, Zhong Chen

*National Key Laboratory of Science & Technology on Multi-spectral Information Processing, Huazhong University of Science and Technology, Wuhan, Hubei 430074, China*

ARTICLE INFO

*Article history:*
Received 2 January 2013
Received in revised form
25 September 2013
Accepted 25 September 2013

*Keywords:*
Average absolute difference
Cytoplasm enhancement
Leukocyte localization
Visual attention

ABSTRACT

In this paper, we propose a fast hierarchical framework of leukocyte localization and segmentation in rapidly-stained leukocyte images (RSLI) with complex backgrounds and varying illumination. The proposed framework contains two main steps. First, a nucleus saliency model based on average absolute difference is built, which locates each leukocyte precisely while effectively removes dyeing impurities and erythrocyte fragments. Secondly, two different schemes are presented for segmenting the nuclei and cytoplasm respectively. As for nuclei segmentation, to solve the overlap problem between leukocytes, we extract the nucleus lobes first and further group them. The lobes extraction is realized by the histogram-based contrast map and watershed segmentation, taking into account the saliency and similarity of nucleus color. Meanwhile, as for cytoplasm segmentation, to extract the blurry contour of the cytoplasm under instable illumination, we propose a cytoplasm enhancement based on tri-modal histogram specification, which specifically improves the contrast of cytoplasm while maintaining others. Then, the contour of cytoplasm is quickly obtained by extraction based on parameter-controlled adaptive attention window. Furthermore, the contour is corrected by concave points matching in order to solve the overlap between leukocytes and impurities. The experiments show the effectiveness of the proposed nucleus saliency model, which achieves average localization accuracy with F1-measure greater than 95%. In addition, the comparison of single leukocyte segmentation accuracy and running time has demonstrated that the proposed segmentation scheme outperforms the former approaches in RSLI.



## 1. Introduction

Differential counting of white blood cells (WBC or leukocytes) plays a crucial role in indicating lots of vital diseases such as hepatitis, leukemia and AIDS (Ghosh et al., 2010). Over the past few years, development of automated cell counter has transferred the time-consuming job from human subjects to automated systems (Bikhet et al., 2000). And it is the cell segmentation that plays a key role in these systems, whose running speed and accuracy are directly influenced by image quality. In image acquisition stage, Wright or Giemsa staining is widely used to facilitate the differentiation of blood cell types. Though traditionally-stained leukocyte images (TSLI) are colored stably with clear details, they have two problems which limit their application. One is the slow dyeing speed, which is not conducive to analyze large numbers of images. The other is the frequent overlap among blood cells (Wang and Wang, 2006), resulting in very time-consuming and challenging segmentation.

To settle the two problems, our team has recently developed a hematology reagent for both rapid leukocyte staining and erythrocyte lysing, which takes only about ten seconds and greatly eliminates the overlap among erythrocytes and leukocytes. However, the dyeing effect is not as good as that of the traditional staining. There are mainly two new problems in rapidly-stained leukocyte images (RSLI). The first is the emergence of substantial dyeing impurities, whose appearances are akin to that of nuclei, makes leukocyte localization difficult. The second is the varying color and illumination, which result in instinct boundaries, become a great challenge in segmentation.

Leukocyte localization is to extract the whole leukocyte from a complicated background. There are many leukocyte localization methods, most of which are realized by thresholding based on a nucleus saliency map (Ghosh et al., 2010; Huang et al., 2012; Jiang et al., 2006; Ko et al., 2011; Kovalev et al., 1995; Madhloom et al., 2010), because the nuclei have the most salient color in TSLI. However, since the nuclei are not the only salient objects in RSLI where dyeing impurities exists, the previous methods failed to precisely locate leukocytes in RSLI.

Segmenting every leukocyte into morphological components such as nucleus and cytoplasm is an essential and important

* Corresponding author. Tel.: +86 027 87559040.
*E-mail addresses:* zxaoyou@gmail.com (X. Zheng), wangyong1989@hust.edu.cn (Y. Wang), gywang@hust.edu.cn, guoyouwang2012@gmail.com (G. Wang).

0968-4328/$ – see front matter © 2013 Elsevier Ltd. All rights reserved.
http://dx.doi.org/10.1016/j.micron.2013.09.006

issue, which attracts the most attention in automatic differential blood counter systems. The pixel-based classification methods, have achieved good segmentation results in TSLI (Fang et al., 2005; Guo et al., 2007; Pan et al., 2012; Theera-Umpon, 2005). However, there is no obvious color difference between cytoplasm and background in RSLI, as well as between nucleus and cytoplasm. With color variation and no spatial information taken into account, these methods cannot get the whole cell region. The boundary-based segmentation methods (Ko et al., 2011; Lin et al., 2005; Sanpanich et al., 2008) are able to get ideal contours in TSLI. However, the cytoplasm boundaries in RSLI are too weak to be precisely obtained.

To sum up, the frequently-used algorithms would not be able to effectively extract and segment each leukocyte in RSLI, for RSLI are more challenging than TSLI. In this paper, we focus on developing a fast and precise leukocyte localization and segmentation approach, which could handle the new problems in RSLI.

## 2. Nucleus saliency model based on average absolute difference (AAD) and Leukocyte localization

RSLI is a complex scene which is flooded with erythrocytes fragments and dyeing impurities, containing a few scattered leukocytes. According to the visual attention mechanism, despite the tiny area of the leukocytes when compared with the whole image and the diversity of color and illumination, human eyes will quickly pick out leukocytes while ignore the others. In RSLI, the impurities and nuclei are both salient objects, very alike in their intensity and color. However, human eye can distinguish nuclei from impurities easily. The main reason is that we know the leukocyte has a round shape, with nucleus lobes in the center. Meanwhile, there is an upper limit to the size of it. Thus there is obvious contrast between nucleus and its local neighborhoods. But the impurities are amorphous and most of them don't possess the local saliency. So we define the average absolute difference (AAD) to enhance nuclei while suppressing impurities. AAD is defined as follows:

$$AAD(x,y) = \max_{\forall \Theta} \left\{ \Delta D | \Delta D = \frac{1}{N_\Omega} \sum_{x,y \in \Omega} I(x,y) - \frac{1}{N_\Theta} \sum_{x,y \in \Theta} I(x,y) \right\} \quad (1)$$

where $\Theta$ and $\Omega$ are the object and background windows as shown in Fig. 1, $N_\Theta$, $N_\Omega$ are the sum of Set $\Theta$ and $\Omega$ respectively, $I(x, y)$ represents the gray-scale of the pixel $(x, y)$. By computing the maximum differences between the surrounding points and the center points, the AAD operator simulates the sensitivity to local spatial discontinuities of visual receptive fields in human visual mechanism to enhance the nuclei. When both Set $\Theta$ and $\Omega$ cover only background, $\Delta D$ is quite small; when only the object is covered in $\Theta$ and $\Omega$ covers the background, $\Delta D$ has the maximal value. Given a fixed $\Omega$, AAD can adaptively find the location of $\Theta$ which shows the maximal contrast between $\Theta$ and $\Omega$. Therefore, $\Theta$ and $\Omega$ can best cover the object and background respectively.

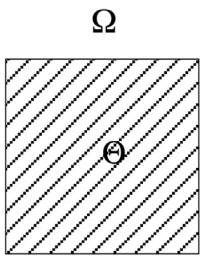


**Fig. 1.** Object and background windows of AAD.

When AAD is used in RSLI, the impurities are restrained effectively while the contrast between nuclei and background is retained, as shown in Fig. 2. Though the impurities are salient in the entire scene, the local contrast is low. So they can be suppressed by AAD when $\Omega$ is a little bigger than the maximum size of leukocytes.

To further suppress noises of small area and make the histogram present a more obvious double-peak, we apply the AAD operator into a well-known saliency model proposed by (Itti et al., 1998). The model is based on a biologically-plausible visual attention architecture which is related to the feature integration theory, explaining human visual search strategies. But this saliency model is not adequately suitable for RSLI because it is in a purely bottom-up manner with no top-down features. According to AAD operator, we make the best use of the two task-dependent features of leukocytes: the darker color of nuclei, the circular shape and the fixed size of leukocyte. Thus the modified saliency model based on AAD is more efficient for detecting nuclei and suppressing impurities. The architecture comparison between the proposed nucleus saliency model and Itti's saliency model is shown in Fig. 3.

The biggest difference between Itti's saliency model and our nucleus saliency model is that the color, intensity and orientation features are replaced by AAD feature in our model. Itti's model is a general model which has to consider different types of features in order to surely include all kinds of salient objects. But for leukocyte localization, we only need to consider the features which can highlight nuclei. Since the nuclei appear dark purple, green channel can best represent the contrast between nuclei and others. In brief, by means of integrating top-down and bottom-up attention, our model is able to perform better than Itti's model. We can see from Fig. 4 that the saliency map gained from our nucleus saliency model can better suppress impurities and highlight nuclei compared with Itti's saliency map.

Another difference is that the purpose of the Itti's model is to shift the focus of attention (FOA) by sorting its saliency, but we just care about the location of each region of interest (ROI) regardless of the saliency order of each ROI So we replace the "winner-take-all" neural network with an automatic binaryzation such as Otsu threshold (Otsu, 1979).

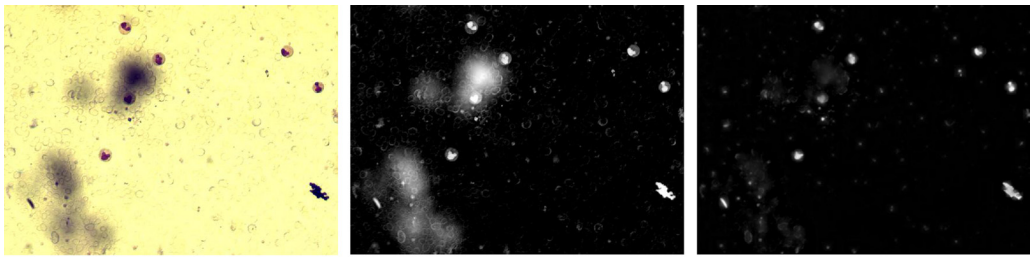


**Fig. 2.** (a) Original image, (b) green channel of (a), (c) AAD map of (b). (For interpretation of the references to color in this figure legend, the reader is referred to the web version of this article.)

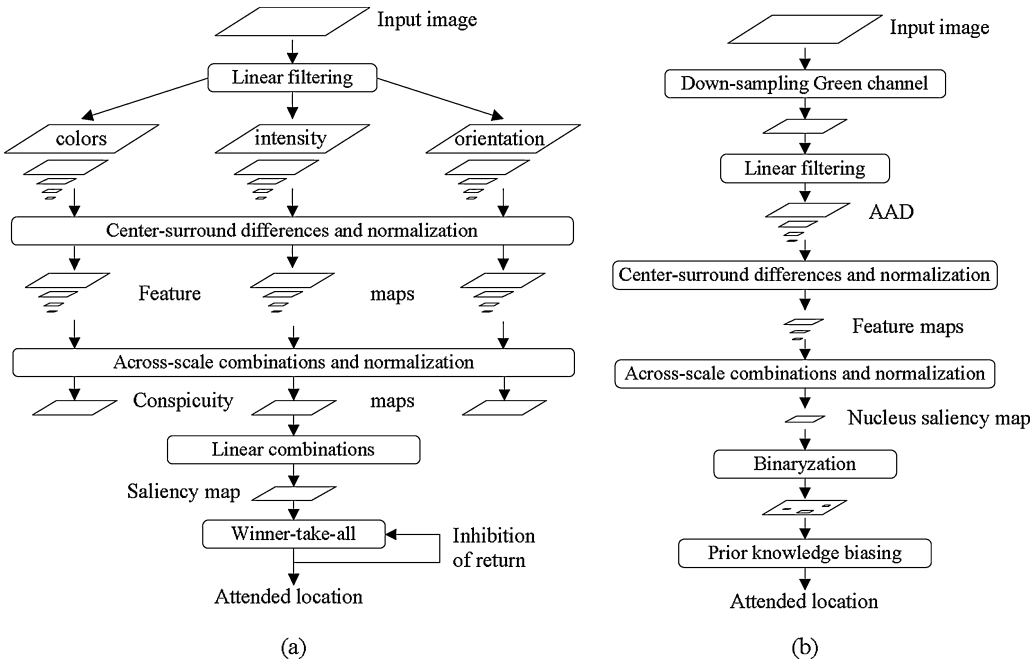


**Fig. 3.** Architecture comparison of saliency models. (a) Itti's model, (b) nucleus saliency model based on AAD.

Using the AAD-based nucleus saliency model, the adaptive saliency window (ASW) is acquired. ASW is a sub-image which is large enough to include all nucleus lobes of each leukocyte. In our scheme, the width and height of each ASW are defined as $(2 \times \mathrm{wn}) \times (2 \times \mathrm{hn})$ centered on the centroid of each salient region $(\mathrm{wn} \times \mathrm{hn})$.

## 3. Leukocyte segmentation within ASW

### 3.1. Preprocessing

Due to instable staining and illumination, the RSLI image quality is poor, which leads to fuzzy edges of nucleus and cytoplasm. Common smoothing filter operators are able to reduce some of the noises, but they can make the weak edges even weaker. In our approach, we found that the mean shift filtering (Comaniciu and Meer, 2002) is more powerful in image edge-preserving than other methods. So the mean shift filtering is used as the smoothing preprocessing, whose steps are as follows:

Step 1. Initialize $j = 1$ and $y_{i,j+1} = x_i$ where $x_i$ is a five-dimensional input in the position $(x, y)$, for example, $x_i = (R, G, B, x, y)$

Step 2. Compute $y_{i,j+1}$ using Eq. (2) until convergence, $y = y_{i,c}$ is the filtered pixel.

$$y_{j+1} = \frac{\sum_{i=1}^{n} x_i g(|y_j - x_i/h|)^2}{\sum_{i=1}^{n} g(|y_j - x_i/h|)^2} \quad j = 1, 2, \ldots \tag{2}$$

where $g(x)$ is the kernel function. By controlling the kernel bandwidth $h = (h_s, h_r)$, we can get different smoothing images. $h = (h_s, h_r)$ is set as $(10, 20)$ where the smoothing effect and time cost are comprehensively considered. Fig. 5 shows some ASWs after mean-shift smoothing.

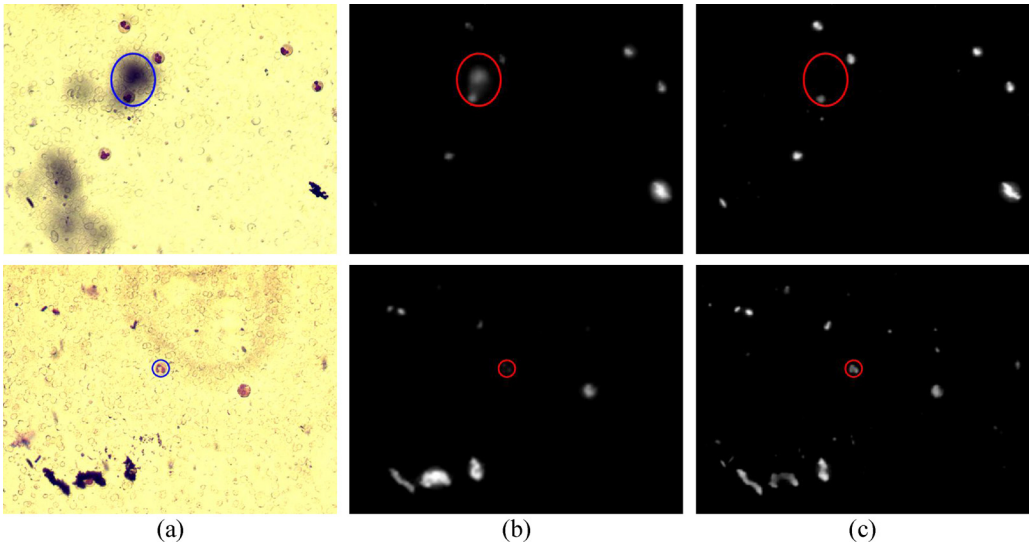


**Fig. 4.** Comparison of saliency maps. (a) Original image, (b) saliency map generated by Itti's model, (c) saliency map yielded by our model.

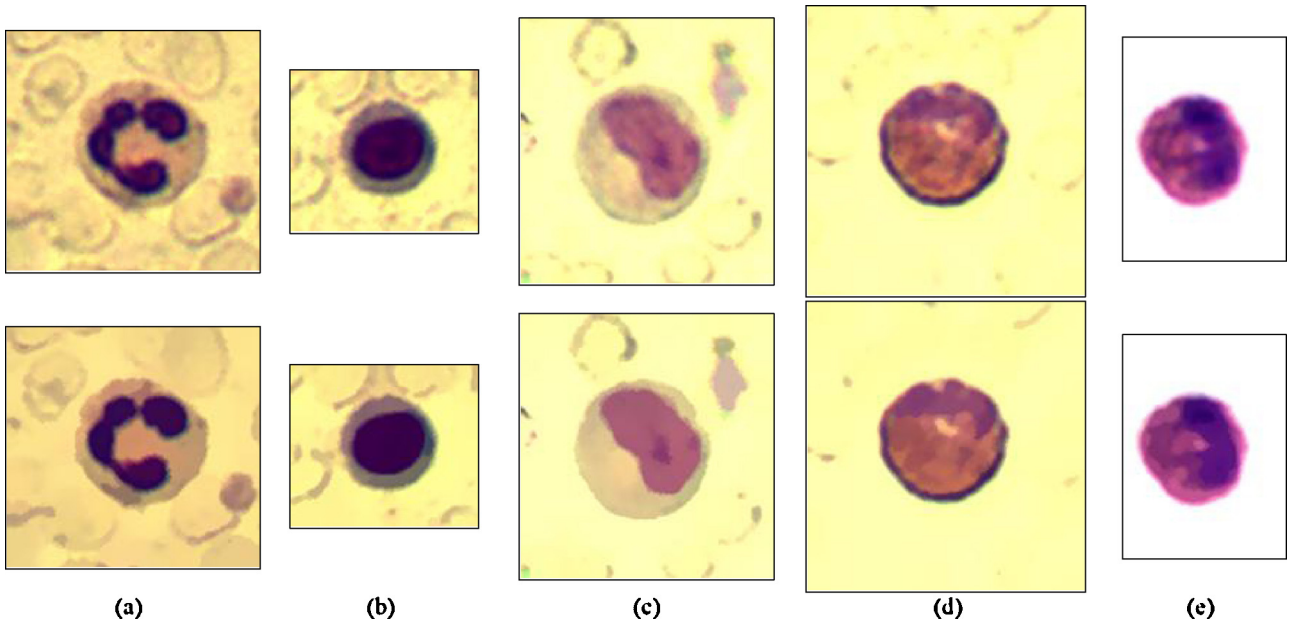


**Fig. 5.** ASW (the top row) and its corresponding mean-shift smoothed image (the bottom row) for five different types of leukocyte: (a) neutrophil, (b) lymphocyte, (c) monocyte, (d) eosinophil and (e) basophil.

### 3.2. Nucleus region segmentation

Though we have already transformed an entire leukocyte image into several ASWs in the last section, there might be one or more leukocytes or impurities within each ASW. In addition, there might still be overlap among leukocytes or between leukocytes and impurities within an ASW, which is not suitable for the single cell segmentation. Although the overlap will exist among leukocytes, the nucleus lobes of different leukocytes do not overlap each other. Besides, it is easier to segment the nucleus than the whole cell. Thus we take a two-step process to segment leukocyte regions and get sub-images simultaneously, and each sub-image contains only one leukocyte. First, all the nucleus lobes in ASW are segmented, and then the nucleus lobes belonging to the same leukocyte are grouped.

#### 3.2.1. Nucleus lobes segmentation inside ASW

Note that the boundaries of nuclei in RSLI are more blurry than TSLI, so we obtain nucleus lobes by watershed algorithm which has a good response to weak edges. Vincent and Soille (1991) gave an algorithmic definition by simulating immersion. As shown in Fig. 6, a gray-scale image $I$ is considered as a topographic surface. It is imagined that the landscape is immersed in a lake, with holes pierced in the local minima. Starting from the minima of lowest altitude, the water will progressively fill up the different catchment basins of $I$. When water coming from different minima meets, dams are built. However, watershed segmentation will produce over segmentation resulting in many meaningless small regions unless it is combined with a good merging algorithm. Thus, we merge the adjacent small regions by defining a color similarity measured by the distance in the CIE Lab color space as follows:

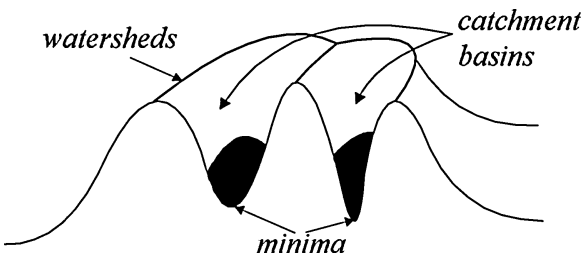


**Fig. 6.** Schematic diagram of watershed transform.

$$D(i,j) = |I_i - I_j| \tag{3}$$

where $I_i$ is the mean vector of color space of the region $R_i$. When the distance between $R_i$ and $R_j$ is small enough (for example, $D(i, j) < 10$), it indicates that the two regions are similar enough in color to be merged as one.

The over segmentation is reduced greatly after region merging based on color similarity rule, but still we are not able to obtain the accurate nucleus lobes here. According to the fact that the nuclei are the most salient objects in the images, histogram contrast (HC) map based on histogram contrast proposed by Ming-Ming et al. (2011) is adopted as the nucleus saliency map to refine the watershed segmentation results. The saliency value of each pixel in HC map is defined as:

$$S(I_k) = S(c_k) = \sum_{j=1}^{n} f_j D(c_k, c_j) \tag{4}$$

where $c_k$ is the color value of pixel $I_k$, $n$ is the number of distinct pixel colors, $f_j$ is the probability of pixel color $c_j$ in image $I$, and $D(i, j)$ is the color distance metric defined in Eq. (4).

Then, an adaptive threshold ($T_\alpha$) value is determined as two times the mean saliency of a given image:

$$T_\alpha = \frac{\alpha}{W \times H} \sum_{x=0}^{W-1} \sum_{y=0}^{H-1} HC(x,y) \tag{5}$$

If the average saliency of each region $S_i > T_\alpha$, the region is considered as nucleus regions. Based on vast experimental data, we set $\alpha = 2$. The flow diagram of the nucleus lobes segmentation within each ASW is illustrated in Fig. 7. And Fig. 8 shows some results of the proposed nuclei segmentation compared with doctors' manual segmentation.

#### 3.2.2. Nucleus lobes grouping inside ASW

To judge whether the nucleus lobes belong to the same leukocyte or not, a nucleus lobes grouping method is needed. To

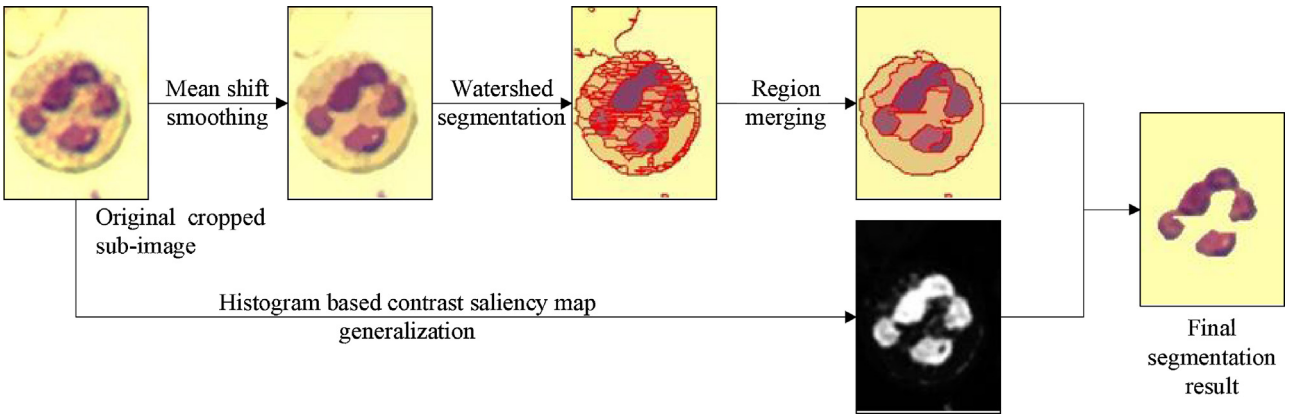


**Fig. 7.** The process of nucleus segmentation.

accomplish nucleus grouping we have used the following shape parameters: the centroid of blob, blob area, centroid distance, minimum distance and maximum distance between two blobs. The centroid distance between blob $B_i$ and blob $B_j$ is defined as follows:

$$d_g(i,j) = ||g_i - g_j|| \tag{6}$$

where $g_i$ is the centroid of blob $B_i$, and $||\cdot||$ is the Euclidean distance.

The definition of minimum and maximum distance between two blobs $B_i$ and $B_j$ is clarified as follows:

$$d_{\min}(i,j) = \min ||C_i - C_j|| \tag{7}$$

$$d_{\max}(i,j) = \max ||C_i - C_j|| \tag{8}$$

where $C_i$ is the pixels on the contour of $B_i$.

And the algorithm in detail is outlined in the following flowchart (Fig. 9) and described as follows:

**Step 1.** If $Area(B_i) > AreaTh1$ and $Area(B_i) > AvgArea$, the blob $B_i$ is marked as an elect blob and added to elect blob list (EBL); otherwise the blob $B_i$ is marked as a candidate blob and added to candidate blob list (CBL). In addition, if EBL is empty, the biggest blob is labeled as an elect blob and added to EBL;

**Step 2.** Compute three distances in Eqs. (6)–(8) between each blobs $C_i$ in CBL and the nearest blob $E_j$ in EBL.

If blob $C_i$ cannot meet both $d_{\min}(C_i, E_j) < DistTh1$ and $d_{\max}(C_i, E_j) < DistTh2$, it is treated as a new elect blob and added into EBL while deleted from CBL.

Otherwise, judge the area size of $C_i$:if $Area(C_i) < AreaTh2$, then blob $C_i$ is merged into the elect blob $E_j$;otherwise, blob $C_i$ is treated as a new blob in EBL and deleted from CBL.where $AreaTh1$ is the minimum size of the biggest nucleus blobs and $AreaTh2$ is the maximum size of the second biggest nucleus blobs. $DistTh1$ and $DistTh2$ are the maximum of the minimum distance and maximum distance between two adjacent nucleus blobs respectively.

After nucleus lobes grouping and region growing inside ASW, we get sub images which are called cell adaptive saliency window (CASW) whose width and height are defined as $(2\,wn) \times (2\,hn)$ centered on the centroid of each blobs region $(wn \times hn)$ belonging to one leukocyte. After finishing this step, the overlapped cells can be separated naturally.

### 3.3. Leukocyte contour extraction within CASW

Since the color of impurities and erythrocyte fragments is similar to that of the adjacent cytoplasm, and the boundaries of cytoplasm is weak, we design a three-step process to extract the cytoplasm contour: firstly, enhance the contrast of cytoplasm; secondly, extract the contour of the overlapped object, which contains the undesired parts and cytoplasm; thirdly, correct the contour to separate the undesired parts.

#### 3.3.1. Cytoplasm enhancement based on tri-modal histogram specification (THS)

Due to the varying illumination, the edge of the cytoplasm is blurry, which makes the contour extraction difficult. It is important to enhance the contrast of the cytoplasm before contour extraction. Histogram-based contrast enhancement is widely used for enhancing contrast, for example, histogram equalization (HE) and adaptive histogram equalization (AHE) (Stark, 2000). However, they cannot specifically enhance the contrast of cytoplasm, and may result in an excessively enhanced output image or reduce the contrast between cytoplasm and background. We propose an enhancement operator based on tri-modal histogram specification (THS), which can enhance the contrast of cytoplasm while suppressing noise.

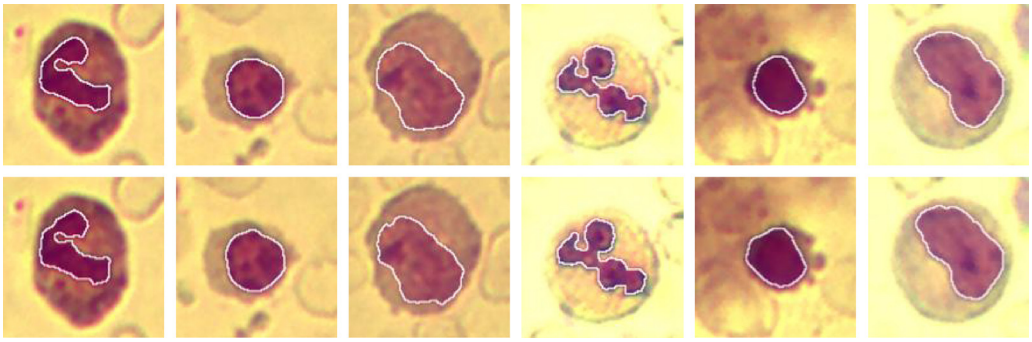

**Fig. 8.** Some nuclei segmentation results compared with pathologists' segmentation. The first row is the results drawn by pathologists. The second row is results of the proposed method.

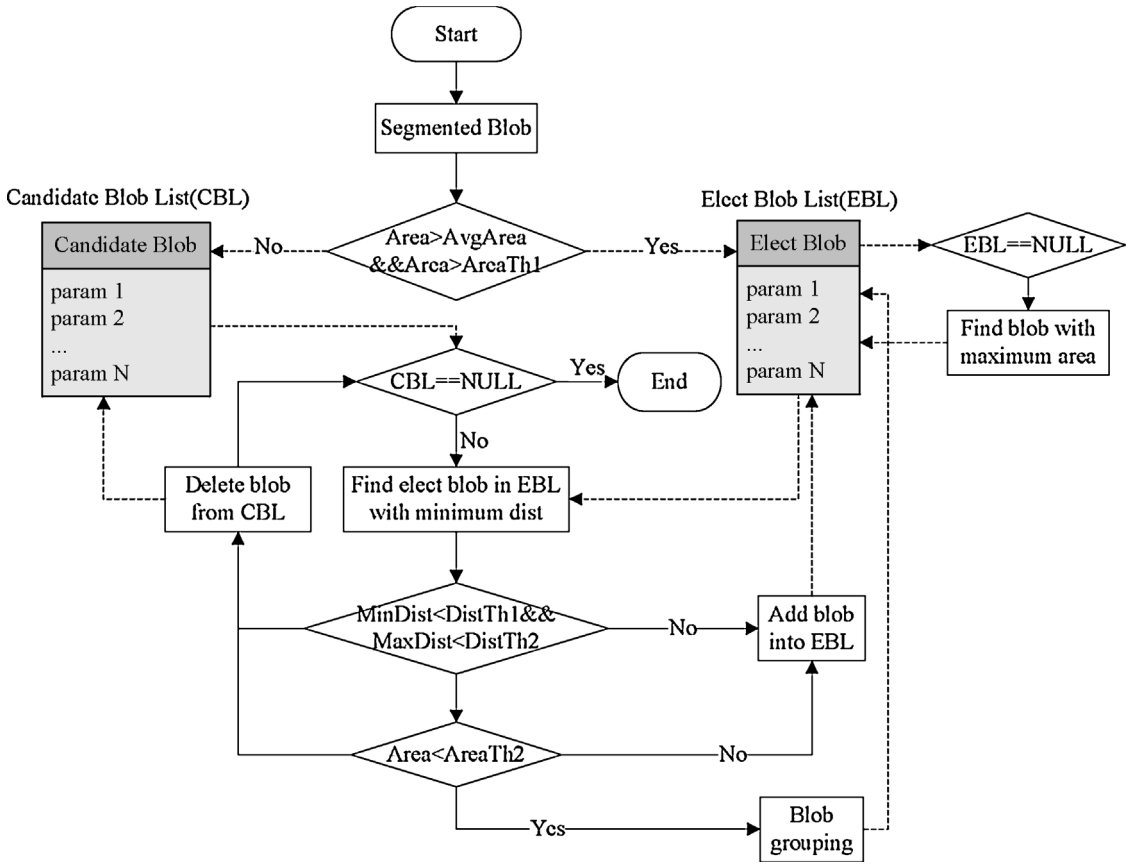


**Fig. 9.** Flowchart of nucleus blobs grouping within ASW.

In an ideal case, the gray histogram of a CASW will follow tri-modal distribution. But actually, it is hard to discriminate cytoplasm from background owing to the unstable and unsuitable illumination. If we could translate the histogram into an ideal tri-modal one, the clustered parts of histogram can be stretched. Consequently, we propose a cytoplasm enhancement based on THS. The steps are as follows:

**Step 1.** Smooth the histogram by scale-space filtering (Carlotto, 1987) with variance σ.

$$F(x,\sigma)=f(x)*g(x,\sigma)=\int_{-\infty}^{\infty}f(u)\frac{1}{\sqrt{2\pi}\sigma}\left[\frac{-(x-u)^2}{2\sigma^2}\right]du \tag{9}$$

where $f(x)$ is a continuous signal, $\sigma$ is the scale, $*$ denotes convolution with respect to $x$.

**Step 2.** Calculate the number ($N$) of pairs of zero-crossings in the second derivative, which can be calculated by:

$$F_{xx}(x,\sigma)=\frac{\partial^2}{\partial x^2}[F(x,\sigma)] \tag{10}$$

**Step 3.** If $N\geq 3$, let $\sigma=\sigma+\delta\sigma$ and return to Step 1; otherwise, stop smoothing.

**Step 4.** Use the ideal histogram as the histogram specification function, and the mapping function is as follows:

$$c(k)=\sum_{j=0}^{k}p(j)=\sum_{j=0}^{k}\frac{n_j}{n}\quad k=0,1,2,\ldots,L-1 \tag{11}$$

where $n$ is the total number of pixels of the image, $n_j$ is the number of occurrences of gray level $j$, and $L$ is the total number of gray levels. Fig. 10(c) shows that HE results in an excessively enhanced output image, in which the noise was enhanced as well. Fig. 10(d) shows that AHE, while quite useful for restraining noise, is not efficient in maintaining the uniformity of cytoplasm. From Fig. 10, we can apparently observe that the proposed CE provides the most efficient cytoplasm enhancement results.

### 3.3.2. Cytoplasm extraction based on parameter-controlled adaptive attention window (PCAAW)

Thanks to the rapid staining, most of the erythrocytes are lysed. Besides, the contrast of cytoplasm is enhanced by the proposed CE in the last section. Thus, it is much easier for us to extract the contour of cytoplasm in RSLI than in TSLI. To achieve fast and precise contour extraction, we propose the extraction method based on the parameter-controlled adaptive attention window (PCAAW), which improves the adaptive attention window (AAW) extraction. AAW extraction proposed by Ko et al. (2009) is a region-based segmentation method based on visual attention with good results in nucleus region extraction. But it can only be used in extracting nucleus, for the color and intensity contrast between nucleus and cytoplasm is higher than that between cytoplasm and background. PCAAW is more suitable for cytoplasm extraction than AAW, and it consists of two steps: initial AAW (IAAW) generation and quad-tree splitting.

*3.3.2.1. IAAW generation.* **Step 1.** Estimate the average intensity $\overline{I_{Cyto}}$ of cytoplasm region and assign new value to the whole nucleus region, in order to yield the luminance map $L$.

$$L(x,y)=\begin{cases}I(x,y), & x,y\notin Nuc\\ \dfrac{1}{W\times H}\displaystyle\sum_{x,y\in CASW}[I(x,y)<Th], & x,y\in Nuc\end{cases} \tag{12}$$

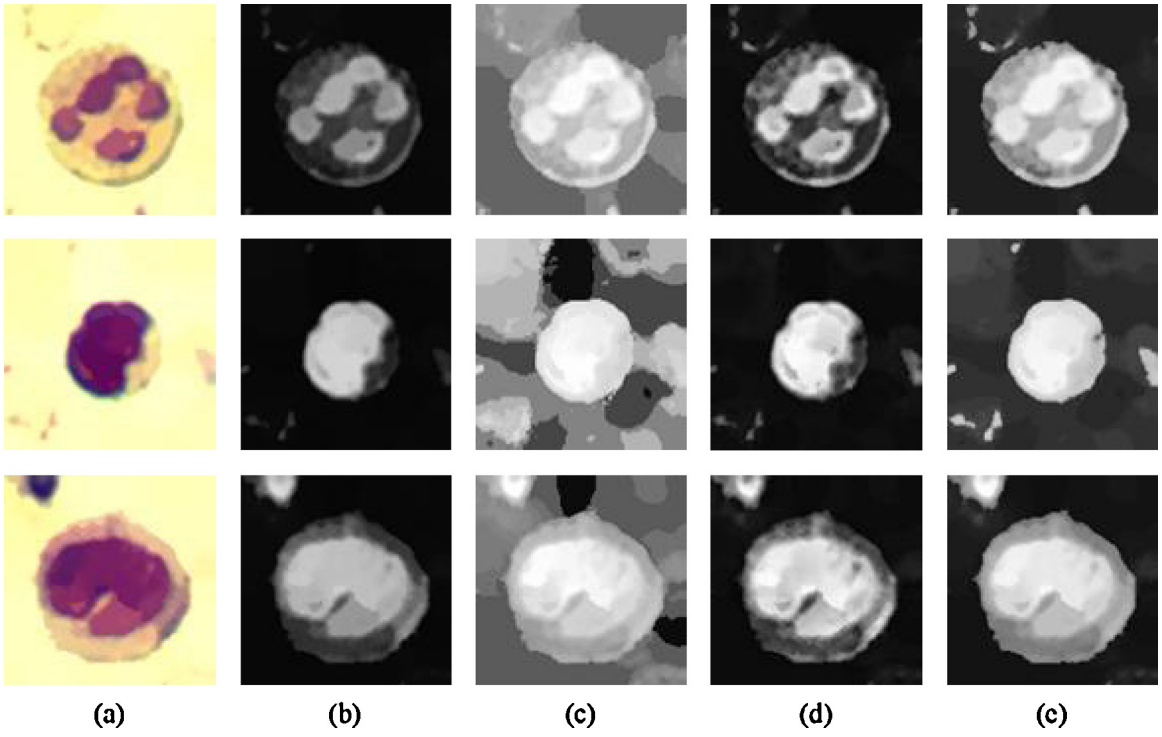


**Fig. 10.** Cytoplasm enhancement (CE) comparison. (a) Smoothed sub images, (b) gray image of (a), (c) HE results of (b), (d) AHE results of (b), (e) CE results of (b).

where $Th$ represents the value using Otsu threshold between 0 and $\overline{I_{Cyto}}/2$.

**Step 2.** Calculate the mean $\bar{L}$ of luminance map.

**Step 3.** Boundary shrinking. If the mean luminance of each side $L_{s_i} > \bar{L}$, or the luminance of certain pixel $L_{s(x,y)} > 2 \times \bar{L}$, then stop shrinking, otherwise keep shrinking. The rectangular region after shrinking is defined as an IAAW.

*3.3.2.2. Quad-tree splitting.* **Step 1.** Set a threshold $\mu_{IAAW} = \frac{1}{N}\sum_{IAAW} L(x,y)$ for block splitting within IAAW.

**Step 2.** Split IAAW into $4 \times 4$ sub-blocks ($S_{b_i}$), let $t = 1$.

**Step 3.** Calculate average $\mu_{b_i} = \frac{1}{N}\sum_{S_{b_i}}(S_{x,y} < S_m)$ for each sub-block.

**Step 4.** If $\mu_{b_i} < \mu_{IAAW}$, then remove the sub-block; Otherwise, re-split $4 \times 4$ sub-block until $\min(W, H) < 4$, let $t = t + 1$ and turn to Step 3.

**Step 5.** Merge blocks and fill hole.

PCAAW improves a lot upon the AAW method. The biggest improvement is that it is more capable of coping with the illumination instability. First, by estimating the gray mean of cytoplasm region and assigning the gray mean of nucleus region, it translates the cytoplasm segmentation into a ROI extraction problem. In this process, the bad influence of nuclei toward cytoplasm segmentation is eliminated. Second, the added shrinking restriction is able to prevent discarding the edge of cytoplasm. The procedures of the cytoplasm contour extraction based on PCAAW are shown in Fig. 11.

*3.3.3. Leukocyte contour correction based on concave points matching (CPM)*

Since the color of impurity and erythrocyte fragments is similar to that of the adjacent cytoplasm, it is common that the erythrocytes fragments or impurities are labeled as a part of the adhesive leukocyte. Though the color and gray features cannot be the separate criteria, the shape features can. Liao and Deng (2002) proposed a contour correction which is fit for circular-shaped leukocytes. However, a considerable part of the leukocytes is not so round. We analyzed the shape features of adhesive regions and found that the pixels on the contour of adhesive parts are concave, and there is a pair of concave points (CP) when entering into and getting out of the adhesive parts. Taking advantage of geometrical features, we proposed a leukocyte contour correction method based on the concave points matching (CPM).

The detection procedure of CP using Freeman chain code (Freeman, 1961) was proposed by Lu and Tong (2002).

First, the absolute chain code using relative chain code as follows:

$$\begin{aligned} &A(0) = 0 \\ &R(i) = ([C(i) - C(i-1) + 8]\bmod 8) > 4 ? R(i) - 8 : R(i) \\ &A(i) = A(i-1) + R(i) \end{aligned} \tag{13}$$

where $C(i)$ is the Freeman chain code of the $i$th point in the contour which is illustrated in Fig. 12, $R(i)$ is the relative chain code, and $A(i)$ is the absolute chain code.

Then the absolute chain code sum of three sequential points is defined as:

$$Sum(i) = A(i) + A(i-1) + A(i-2) \tag{14}$$

Finally, the CCP can be obtained by calculating the difference of chain code sum, which is defined as follows:

$$Diff(i) = Sum(i+3) - Sum(i) \tag{15}$$

The difference of chain code sum is proportional to the curvature, which is able to indicate the CP of a contour. If we go

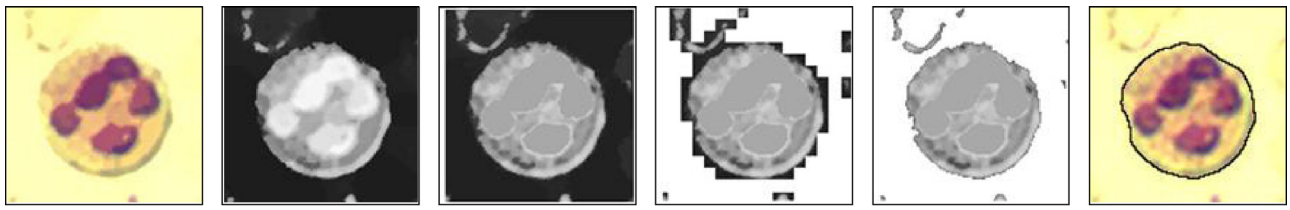


**Fig. 11.** Process of the cytoplasm contour extraction based on PCAAW.

counterclockwise along the contour, the point with negative difference is a concave corner, and the positive difference indicates a convex corner.

CPM process is then utilized to separate the adhesive parts from the cytoplasm. The steps are as follows:

**Step 1.** Find all the CP of contour after smoothing the contour of leukocyte with the Gaussian filter.

**Step 2.** Choose the midpoint of each CP set as the candidate concave point (CCP) of the set. If the number of CCP is more than two, then proceed to Step 3; otherwise, end the steps.

**Step 3.** For each CCP: find the closest N other elect concave points which are treated as the elect concave point (ECP) in order of chain length; and calculate the arc-chord ratio $r_{ij}$ between it and every ECP.

$$r_{ij} = \frac{l_{chain}(i,j)}{d_{euc}(i,j)} \tag{16}$$

where $l_{chain}(i,j)$ is the chain length between point $P_i$ and point $P_j$, and $d_{euc}(i,j)$ is the Euclidean distance between two points. According to experimental data, there are no three or more adhesive parts within a sub-image of individual leukocyte. So $N = 5$.

**Step 4.** If $r_{ij} > 1.5$, we take it as a successful matching, and draw a line through the pair of points to separate the raised part. If the line goes across the nucleus, then give up separation; otherwise, keep the center region of the separated regions as the leukocyte. Fig. 13 shows an example of CPM.

As shown in Fig. 14, the method has a good effect on the separation where there is an obvious pit between principal leukocyte part and overlapped impurities or cells. It should be mentioned that the method would fail if the concavity is not clear. Despite its limitation, this method is able to solve most of the overlap problem in RSLI where most of erythrocytes have been lysed. The framework of the whole leukocyte segmentation scheme is shown in Fig. 15.

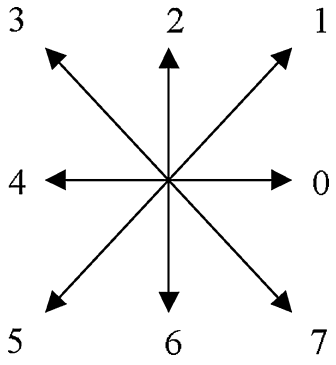


**Fig. 12.** The direction of the eight connected Freeman chain code.

## 4. Experimental results

All the algorithms were implemented with Visual C++6.0 on a Windows XP operating system with a 3.07 GHz Intel Core i3 CPU and 2 GB memory.

In our study, all smears were prepared using rapid staining. The images were taken by a Motic Moticam Pro 252A microscope camera with a N800-D motorized auto-focus microscope, and each image has a size of $2048 \times 1536$ and depth of 24 bits color. The tests consisted of 103 color peripheral blood images and 54 sub-images ($116 \times 116$) of single leukocyte. The color peripheral blood images, which were prepared under three different imaging conditions corresponding to three folders (the first and second folder contained 30 images each and the third one contained 43 images), contain 528 leukocytes. Each sub-image contains a single type of stained leukocytes: 17 neutrophils, 14 lymphocytes, 10 monocytes, 10 eosinophils and 3 basophils. To compare the accuracy of the proposed method and manual method, the golden standard contours of nucleus regions and leukocytes were manually drawn by doctors in Jiangxi Tecom Science Corporation.

### 4.1. Leukocyte localization results

Because of the existence of dyeing impurities caused by rapid staining, the existing algorithms are not suitable for this kind of leukocyte images, and there are no comparative experiments for the proposed leukocyte localization. To assess the performance of the leukocyte localization, we provided Precision ($P$), Recall ($R$) and F1-Measure (F1) to illustrate its accuracy, and running time to declare its real-time capability. $P$, $R$ and F1 are defined as follows:

$$P = \frac{TP}{(TP+FP)}, R = \frac{TP}{(TP+FN)}, F1 = \frac{2P*R}{(P+R)} \tag{17}$$

where $TP$ represents the number of object pixels that are labeled correctly; $FP$ is the number of pixels that should be excluded but are included; $FN$ is the number of pixels that should be included but are excluded. Table 1 shows the performance evaluation results using Eq. (17) and real-time capability. The illumination of the images in the first and the second folders is weak and strong respectively; and the appearing color in the third folder is different from the previous two folders: the background is nearly light purple other than bright yellow. One leukocyte sample of the third folder is shown in the last column in Fig. 17. As shown in Table 1, the average time cost of the proposed leukocyte localization method is less than 300 milliseconds and the average values of F1 is maintained over 95%. It

**Table 1**
Precision, recall and time cost of leukocyte localization.

| Dataset | 1 | 2 | 3 | Average |
|---|---|---|---|---|
| Precision (%) | 84.30 | 92.41 | 95.58 | 91.94 |
| Recall (%) | 98.08 | 99.52 | 100.00 | 99.43 |
| F1-Measure (%) | 90.67 | 95.83 | 97.74 | 95.54 |
| Time cost (ms) | 259.47 | 294.27 | 260.34 | 269.61 |

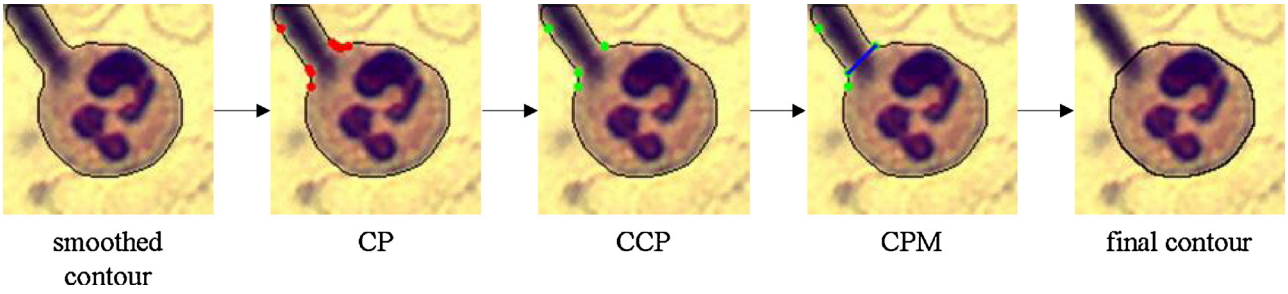


**Fig. 13.** Flowchart of cytoplasm contour correction based on CPM.

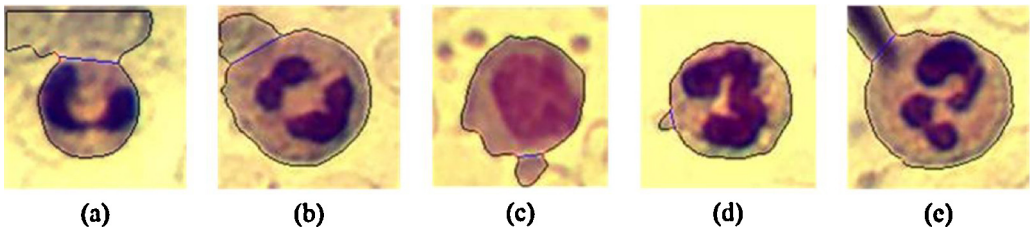


**Fig. 14.** Results of leukocyte contours correction based on CPM.

is obvious that the proposed method produced a good localization performance both in accuracy and time cost.

### 4.2. Comparison of segmentation results in different leukocyte images

In this subsection, we compared (Theera-Umpon, 2005)'s method and (Ko et al., 2011)'s method with the presented method based on 54 leukocyte images.

Theera-Umpon's method used the color features of pixels through FCM to segment the leukocyte into nucleus, cytoplasm and background in the order of ascending gray level. Ko's method used different features to segment nucleus and cytoplasm: first, a saliency map was gotten by the fusion of the probability map using color features and the distance map using region features, and nuclei region was extracted by mean shift clustering based on the saliency map; then to segment cytoplasm, the cell contour was gained by canny edge detector and GVF snake utilizing edge features. The two segmentation methods are two kinds of typical algorithms using different features and have gotten satisfactory effect in single leukocyte segmentation of RSLI.

To evaluate the single leukocyte segmentation performance of each method, the segmentation results of each method were compared with the manually drawn segmentation results by doctors. Two evaluation parameters, F1 of nucleus regions computed by Eq. (17) and relative distance error (RDE) of leukocyte contours computed by Eq. (18) which is proposed by (Yang-Mao et al., 2008), are used to indicate the accuracy of segmentation, and the running time is also compared.

$$RDE = \frac{1}{2}\left(\sqrt{\frac{1}{N_s}\sum_{i=1}^{N_s} d2s_i} + \sqrt{\frac{1}{N_m}\sum_{j=1}^{N_m} d2m_j}\right) \tag{18}$$

where $s_i$ and $m_i$ are the pixels on $s$ and $m$ respectively, $s$ and $m$ are the segmented contour extracted automatically by the algorithm and the ground truth contour extracted by doctors, $N_s$ and $N_m$ are the sum of pixels of $s$ and $m$, $d_{s_i}$ and $d_{m_i}$ are described as:

$$\begin{aligned} d_{s_i} &= \min\{dist(s_i, m_j) | j = 1, 2, \ldots, N_m\} \\ d_{m_i} &= \min\{dist(m_j, s_i) | i = 1, 2, \ldots, N_s\} \end{aligned} \tag{19}$$

where $dist(A, B)$ represents the Euclidean distance between point A and B.

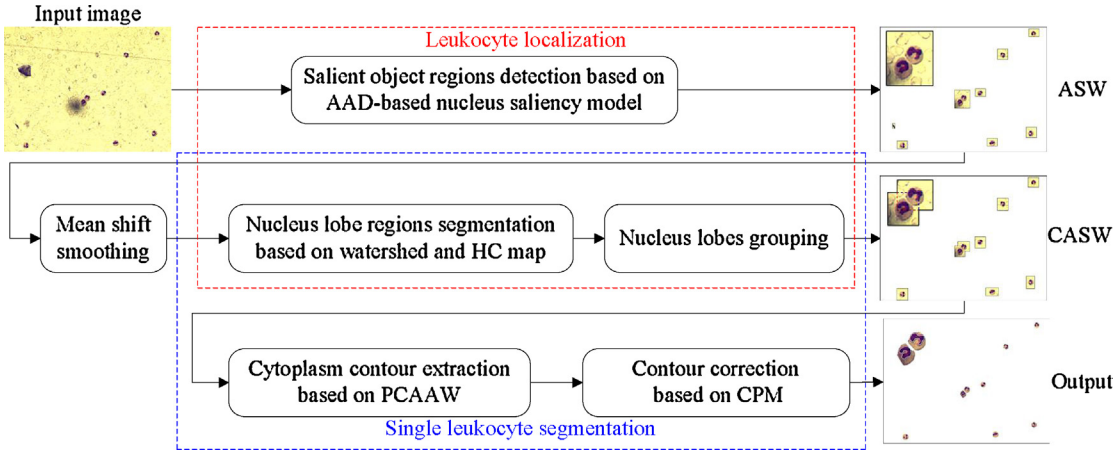


**Fig. 15.** Framework of leukocyte segmentation.

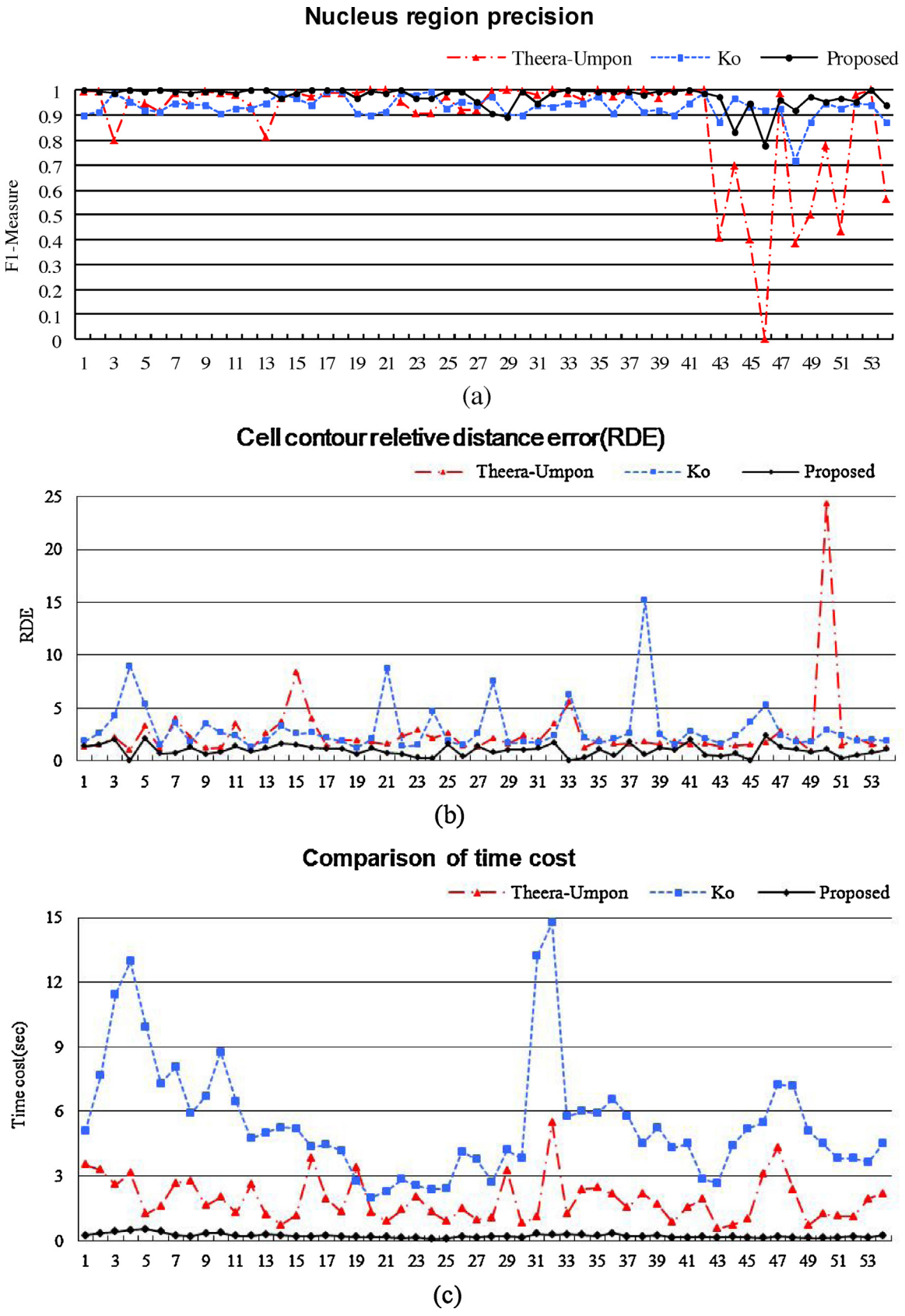


**Fig. 16.** Comparison of segmentation results using proposed method, Theera-Umpon's method and Ko's method. Numbers 1–17 on *X*-axis represent images of neutrphils, 18–31 represent images of lymphocytes, 32–41 represent images of monocytes, 42–51 represent images of eosinophils, and 52–54 represent images of basophils. (a) F1-measure of nucleus segmentation, (b) RDE of cytoplasm segmentation, and (c) total segmentation time.

**Table 2**
Evaluation of segmentation results with 54 images.

| | | Neutrophil | Lymph | Monocyte | Eosinophil | Basophil | Average |
|---|---|---|---|---|---|---|---|
| F1-Measure % | Theera-Umpon's method | 95.20 | 96.72 | 98.93 | 55.99 | 84.89 | 88.45 |
| | Ko's method | 94.40 | 94.46 | 93.84 | 90.75 | 91.99 | 93.50 |
| | Our method | 99.45 | 97.09 | 99.46 | 93.13 | 96.65 | 97.51 |
| RDE | Theera-Umpon's method | 2.60 | 2.03 | 2.24 | 3.94 | 1.65 | 2.58 |
| | Ko's method | 3.11 | 2.90 | 3.95 | 2.67 | 1.94 | 3.06 |
| | Our method | 1.22 | 0.89 | 1.05 | 0.88 | 0.84 | 1.02 |
| Time cost (ms) | Theera-Umpons's method | 2.19 | 1.53 | 2.15 | 1.70 | 1.75 | 1.90 |
| | Ko's method | 7.02 | 3.81 | 6.34 | 4.85 | 4.00 | 5.49 |
| | Our method | 0.31 | 0.17 | 0.23 | 0.15 | 0.19 | 0.22 |

Fig. 16(a) and Table 2 show the nucleus segmentation accuracy of three methods evaluated by Eq. (17). Although the accuracy of Theera-Umpon's method is also very good and the performance in several images is even better than our scheme, it shows a quite poor performance for eosinophils. Ko's method has a lower accuracy and stability than ours though its performance outperforms other algorithms. When comprehensively evaluating the performance of nucleus segmentation method, the existing methods are not as good as the proposed method.

Fig. 16(b) demonstrates that the contours of the whole leukocyte extracted by our method come closest to the ground truth, and the average RDE is near 1.02 compared with 2.58 and 3.06 of Theera-Umpon's method and Ko's method respectively.

The time cost of the three methods is shown in Fig. 16(c). The average speed of the proposed method is about 200ms which is much faster than 1.9 s of Theera-Umpon's method and 5.46 s of Ko's method.

Fig. 17 shows different results of the three methods and the final contours of nuclei (white curve) and cytoplasm (black curve) performing on sampling sub images of five types of leukocytes. As shown in Fig. 17, the dyeing colors are instable, the illuminance is distinctly different, and different types of leukocytes appear different colors both in nucleus and cytoplasm. When compared with other two methods which cannot avoid over-segmentation and under-segmentation, the proposed method was the most robust when processing the instable RSLI with poor illumination.

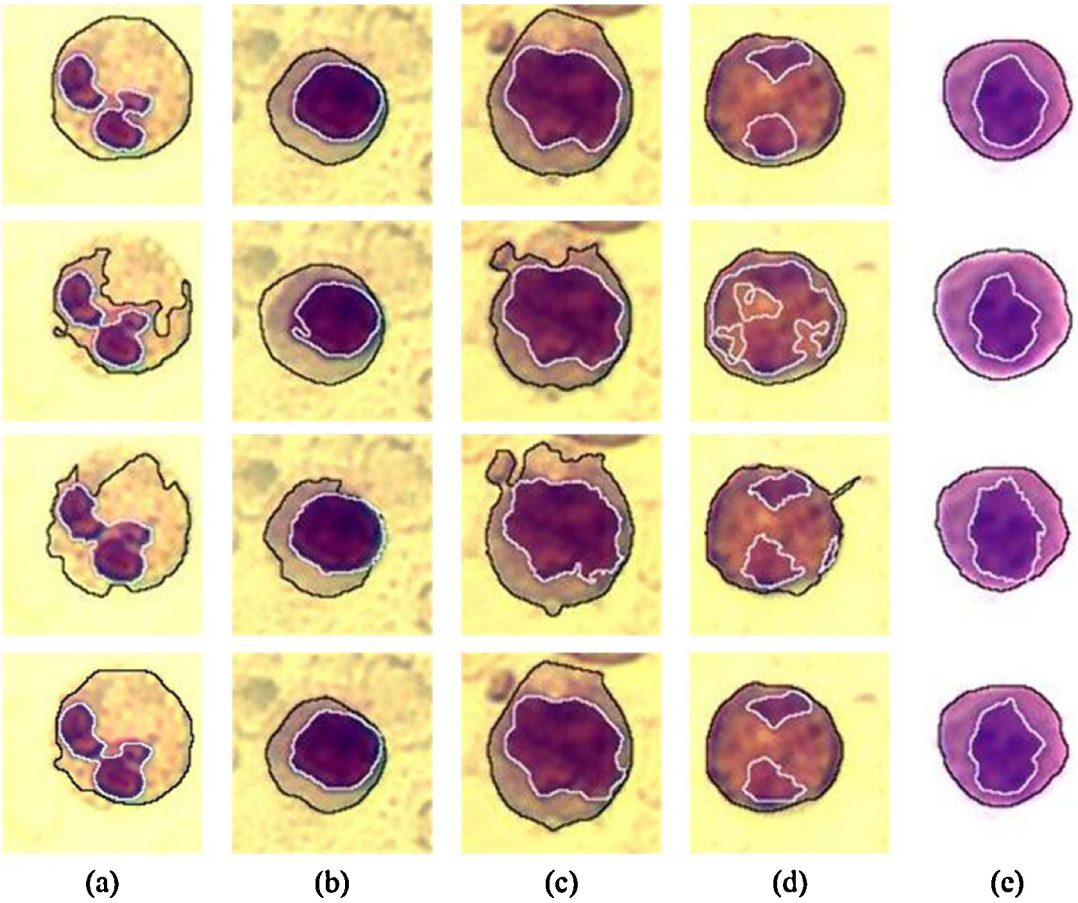


**Fig. 17.** Examples of segmentation results from different methods on sub images of different types of leukocyte. (a) neutrophils, (b) lymphs, (c) monocytes, (d) eosinophils, (e) basophils. The first row is the result of doctors' segmentation, the second row is the result of Theera-Umpon's method, the third row the result of Ko's method and the fourth row is the result of our method.

## 5. Conclusion

Since the rapid staining significantly improves the staining speed and promotes the erythrocyte lysing, it will be a valuable and important work to achieve precise and fast segmentation of the RSLI. Also, it is a difficult and challenging problem because of the complexity of the RSLI, for instance, the containment of dyeing impurities and erythrocyte fragments, color inconsistency, and the overlap among leukocytes and erythrocyte fragments. To solve these problems, this paper presents a complete framework of leukocyte localization and segmentation based on the visual saliency attention mechanism. First, the AAD-based nucleus saliency model effectively solves the leukocyte localization problem despite strong disturbances of dyeing impurities and uncertain conditions of color and illumination. Then, two different segmentation schemes are processed to extract nucleus and cytoplasm regions separately, which eliminate the bad influence of illumination inconsistency and edge blurring. Furthermore, the problem of overlap between leukocytes and impurities (or erythrocyte fragments) is also successfully settled. The nucleus lobes grouping and the contour correction stepwise separate leukocytes from impurities. Experiments indicate that the proposed localization and segmentation method owns low time cost, good accuracy and strong robustness against varying illumination and unstable color.

Combined with the rapid staining, the proposed method could be used in automated leukocyte counting systems more widely. In addition to RSLI, the proposed techniques can also have a reference value for the cell detection and segmentation of other kinds of images as well, for example, TSLI and cervical smear images. Based on the proposed method, we intend to develop an automated cell counter which will include abnormal leukocyte analysis, feature extraction and classifying the leucocytes into five categories in future work.

## References


Bikhet, S.F., Darwish, A.M., Tolba, H.A., Shaheen, S.I., 2000. Segmentation and classification of white blood cells. In: Proceedings of the IEEE International Conference on Acoustics, Speech, and Signal Processing, pp. 2259–2261.

Carlotto, M.J., 1987. Histogram analysis using a scale-space approach. IEEE Transactions on Pattern Analysis and Machine Intelligence 9, 121–129.

Comaniciu, D., Meer, P., 2002. Mean shift: a robust approach toward feature space analysis. IEEE Transactions on Pattern Analysis and Machine Intelligence 24, 603–619.

Fang, Y., Zheng, C., Pan, C., Liu, L., 2005. White blood cell image segmentation using on-line trained neural network. In: Proceeding of the 27th IEEE International Conference on Engineering in Medicine and Biology Society, pp. 6476–6479.

Freeman, H., 1961. On the encoding of arbitrary geometric configurations. IRE Transactions on Electronic Components Parts 10, 260–268.

Ghosh, M., Das, D., Chakraborty, C., Ray, A.K., 2010. Automated leukocyte recognition using fuzzy divergence. MICRON 41, 840–846.

Guo, N.N., Zeng, L.B., Wu, Q.S., 2007. A method based on multispectral imaging technique for white blood cell segmentation. Computers in Biology and Medicine 37, 70–76.

Huang, D.C., Hung, K.D., Chan, Y.K., 2012. A computer assisted method for leukocyte nucleus segmentation and recognition in blood smear images. Journal of Systems and Software 85, 2104–2118.

Itti, L., Koch, C., Niebur, E., 1998. A model of saliency-based visual attention for rapid scene analysis. IEEE Transactions on Pattern Analysis and Machine Intelligence 20, 1254–1259.

Jiang, K., Liao, Q.M., Xiong, Y., 2006. A novel white blood cell segmentation scheme based on feature space clustering. Soft Computing 10, 12–19.

Ko, B., Seo, M., Nam, J.Y., 2009. Microscopic cell nuclei segmentation based on adaptive attention window. Digital Imaging 22, 259–274.

Ko, B.C., Gim, J.W., Nam, J.Y., 2011. Automatic white blood cell segmentation using stepwise merging rules and gradient vector flow snake. MICRON 42, 695–705.

Kovalev, V.A., Grigoriev, A.Y., Ahn, H., Myshkin, N.K., 1995. Automatic localization and feature extraction of white blood cells. In: Proc. SPIE 2434 Medical Imaging, pp. 754–765.

Liao, Q., Deng, Y., 2002. An accurate segmentation method for white blood cell images. In: Proceedings of the IEEE International Symposium on Biomedical Imaging, pp. 245–248.

Lin, Y., Meer, P., Foran, D.J., 2005. Unsupervised segmentation based on robust estimation and color active contour models. IEEE Transactions on Information Technology in Biomedicine 9, 475–486.

Lu, Z.Q., Tong, T., 2002. The application of chain code sum in the edge form analysis. Journal of Image and Graphics 7, 1323–1328.

Madhloom, H.T., et al., 2010. An automated white blood cell nucleus localization and segmentation using image arithmetic and automatic threshold. Journal of Applied Sciences 11, 959–966.

Ming-Ming, C., Guo-Xin, Z., Mitra, N.J., Xiaolei, H., Shi-Min, H., 2011. Global contrast based salient region detection. In: IEEE Conference on Computer Vision and Pattern Recognition (CVPR), pp. 409–416.

Otsu, N., 1979. A threshold selection method from gray-level histograms. Systems, IEEE Transactions on Man and Cybernetics 9, 62–66.

Pan, C., Park, D.S., Yoon, S., Yang, J.C., 2012. Leukocyte image segmentation using simulated visual attention. Expert Systems with Applications 39, 7479–7494.

Sanpanich, A., Iampa, W., Pintavirooj, C., Tosranon, P., 2008. White blood cell segmentation by distance mapping active contour. In: International Symposium on Communications and Information Technologies, pp. 251–255.

Stark, J.A., 2000. Adaptive image contrast enhancement using generalizations of histogram equalization. IEEE Transaction on Image Processing 9, 889–896.

Theera-Umpon, N., 2005. White blood cell segmentation and classification in microscopic bone marrow images. Lecture Notes in Computer Science 3614, 787–796.

Vincent, L., Soille, P., 1991. Watersheds in digital spaces: an efficient algorithm based on immersion simulations. IEEE Transactions on Pattern Analysis and Machine Intelligence 13, 583–598.

Wang, S., Wang, M., 2006. A new detection algorithm (NDA) based on fuzzy cellular neural networks for white blood cell detection. IEEE Transactions on Information Technology in Biomedicine 1, 5–10.

Yang-Mao, S.F., Chan, Y.K., Chu, Y.P., 2008. Edge enhancement nucleus and cytoplast contour detector of cervical smear images. IEEE Transactions on Systems, Man, Cybernetics, Part B 38, 353–366.